Pergamon

Int. J. Heat Mass Transfer. Vol. 40, No. 9, pp. 2187–2199, 1997

0017–9310/97 $17.00+0.00

PII: S0017–9310(96)00248–7

The dual influence of curvature and buoyancy in fully developed tube flows

D. J. GOERING
Department of Mechanical Engineering, University of Alaska, Fairbanks, AK 99775, U.S.A.

J. A. C. HUMPHREY
Department of Aerospace and Mechanical Engineering, University of Arizona, Tucson, AZ 85721, U.S.A.

and

R. GREIF
Department of Mechanical Engineering, University of California, Berkeley, CA 94720, U.S.A.

(*Received* 9 *January* 1996 *and in final form* 24 *June* 1996)

Abstract—Fully developed laminar flow through a heated horizontal curved tube is studied using a two-dimensional numerical representation of the fully-elliptic Navier–Stokes and energy equations. Buoyancy and curvature effects are included and two types of thermal boundary conditions are examined. Heat transfer and pressure drop data are provided in addition to flow velocity and temperature contours. Regime maps are presented which delineate the range of combined curvature/buoyancy influence for both types of boundary conditions. The results for uniform peripheral heat flux reveal a large region of parameter space where fully developed laminar solutions could not be found. © 1997 Elsevier Science Ltd. All rights reserved.

1. INTRODUCTION

The flow fluids through curved and/or heated tubes has been of theoretical and practical interest for many years. Body forces arising from tube curvature and buoyancy generate complex cross-stream motions which act to increase momentum and energy transport from the tube walls while decreasing axial (streamwise) dispersion. These features have led to the use of curved tubes in compact heat exchangers and as chemical reactors.

In addition to their practical importance, curved and buoyant tube flows are of considerable theoretical interest because of the complexity of the secondary motions which arise within them. In each case the laminar Poiseuille flow corresponding to a straight tube flow is modified by transverse body forces that generate cross-stream motions. Tube curvature induces secondary motion by way of the imbalance between the centrifugal acceleration and the radial pressure gradient. In heated tubes the secondary motion is generated by density differences arising between fluid near the wall and fluid in the central region of the tube cross section.

The analysis of Dean [1, 2] showed that the parameter characterizing secondary motion in curved tube flow for small curvature ratios is the Dean number, De. A similar analysis for buoyant flow in heated straight tubes was carried out by Morton [3] who showed that the modified Grashof number, Gr, is the dynamical parameter which characterizes secondary motion in this configuration. With reference to Fig. 1, the present study is concerned with fully developed flow in horizontal heated curved tubes which may be affected by both curvature and buoyancy. For large Dean and small Grashof numbers, the influence of curvature will dominate the cross-stream motion and determine the global characteristics of the flow. However, for small Dean and large Grashof numbers, buoyancy will play the dominant role. For both of these cases data are available from many previous studies which have examined the impact of either buoyancy or curvature alone. For the intermediate range, where the values of De and $Gr^{1/2}$ are comparable in value, both curvature and buoyancy are important. We refer to this as the range of 'dual influence'. For the heated horizontal curved tube configuration, the effect of curvature is to cause the fluid at the tube center to move towards the outer radius wall with a return flow along the top and bottom walls

NOMENCLATURE

a	tube radius
f_c/f_s	friction ratio
g	gravitational acceleration
k	thermal conductivity
p	pressure
q	heat flux
r	radial coordinate
u	radial velocity component
v	circumferential velocity component
w	axial velocity component
$\bar{w}$	bulk average axial velocity
De	Dean number, $Re(\delta)^{1/2}$
G_c/G_s	pressure gradient ratio
Gr	Grashof number, $(\beta g \tau a^4/\nu^2)$ $Re\,Pr$ or $2\beta g q w a^4/\nu^2 k$
Nu	Nusselt number
Pe	Peclet number, $RePr$
Pr	Prandtl number, α/ν
R_c	curvature radius
Re	Reynolds number, $2a\bar{w}/\nu$
T	temperature
T_b	bulk temperature
$\bar{T}_w$	peripherally averaged wall temperature.

Greek symbols

α	thermal diffusivity
β	coefficient of thermal expansion
δ	curvature ratio, a/R_c
μ	dynamic viscosity
ν	kinematic viscosity
ϕ	angular coordinate in circumferential direction
ρ	fluid density
τ	axial temperature gradient
θ	angular coordinate in axial direction.

Subscripts

f	fluid property
o	reference quantity
r	radial component
w	quantity at tube wall
ϕ	ϕ component.

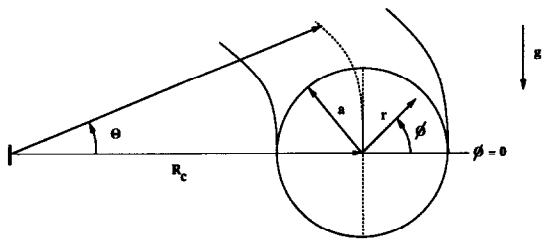

Fig. 1. Horizontal curved tube geometry represented by toroidal coordinates r, θ, and ϕ.

of the tube. The effect of buoyancy is to cause the fluid to rise (or fall) along the side walls of the tube and to fall (or rise) along the vertical centerline of the tube cross section.

Very few studies have attempted to characterize the combined effects of curvature and buoyancy in curved tube flows. The study of Cheng and Yuen [4] provided flow visualization pictures of the cross-stream motion, although it is not clear whether this was done in the fully developed region. Yao and Berger [5] used perturbation methods to obtain solutions for fully developed buoyant flow in horizontal and vertical coils. Prusa and Yao [6] extended this work using a numerical procedure for the horizontal case and provided the first data for the range of dual influence, including a regime map which showed the location of the dual influence region in De–Gr parameter space. Lee *et al.* [7] used a numerical technique which employed a hybrid differencing scheme (a combination of central and first order upwind differencing) for the convective terms, to examine the dual influence regime at higher parameter values. Finally, Futagami and Aoyama [8] completed another numerical study of the dual influence range which examined the effect of the Prandtl number. Both Lee *et al.* and Futagami and Aoyama produced extended flow regime maps for the dual influence region.

All of the numerical studies cited above were limited to the case where the total cross-sectional heat flux is constant and the tube wall temperature is uniform in the peripheral direction, referred to as condition 1 in the present study. Under these conditions the tube wall temperature is a function of the axial coordinate only ($T_w = f(\theta)$), while the heat flux normal to the tube wall varies in the peripheral direction ($q_w = f(\phi)$). In the present study, condition 1 is examined in addition to the case of uniform peripheral heat flux ($q_{w,\phi} = \text{const.}$), referred to as condition 2. For condition 2 the tube wall temperature varies in both the axial and peripheral directions ($T_w = f(\theta, \phi)$) and the wall heat flux is constant in both the peripheral and axial directions. Other than the early study by Newell and Bergles [9] who examined buoyant straight-tube flow with both types of conditions, very little data are available for condition 2, and there appears to be none for curved tubes. This is true despite the wide applicability of condition 2 (e.g. low thermal conductivity tubes exposed to a uniform heat flux). This study presents results for the heat transfer and friction of heated curved tube flow with boundary conditions 2, and also presents a regime map which delineates the dual influence region where both buoyancy and

curvature are important for this condition. These results shows dramatically different flow characteristics for the two conditions, including a large region of *De–Gr* parameter space where *no fully developed solutions* could be found for condition 2.

In addition to providing data for boundary condition 2, the present work also attempts to resolve conflicts which currently exist in the literature for condition 1. Examination of the regime maps provided in the studies of Prusa and Yao, Lee *et al.*, and Futagami and Aoyama reveals disagreement in the range of dual influence. This difficulty was pointed out and discussed by Lee *et al.* but was not addressed by Futagami and Aoyama. In Section 4.3 we re-examine this issue and attempt to provide insight on this point.

2. CONSERVATION EQUATIONS AND BOUNDARY CONDITIONS

The motion of fluids through heated curved tubes is conveniently described by the conservation equations for mass, momentum and energy written for the toroidal coordinate system shown in Fig. 1. In this work we consider only curved tubes which are oriented horizontally with respect to the gravity vector, resulting in curvature and buoyancy body forces which act in the horizontal and vertical directions, respectively. The coordinate directions are defined as r, the radial distance from the tube center, ϕ, the poloidal angle and θ, the toroidal angle. Fluid properties are assumed to be constant and buoyancy is included in the momentum equations where the Boussinesq approximation is used. Non-dimensional variables are defined as follows:

$$r=\frac{r'}{a}\quad \theta=\frac{\theta'}{\delta Re}\quad T=\frac{T'}{\frac{1}{2}RePra\tau}$$

$$u=\frac{u'a}{\nu}\quad v=\frac{v'a}{\nu}\quad w=\frac{w'}{\bar{w}}\quad p=\frac{p'}{\rho\bar{w}^2}$$

where the primed quantities are dimensional and u, v, and w are the velocity components in the r, ϕ, and θ directions, respectively. Note that the poloidal angle ϕ is used directly without scaling. Also, note that this non-dimensionalization results in cross-stream velocities (u,v) which scale with De and/or $Gr^{1/2}$. The ratio Gr/De^2 indicates the relative importance of buoyancy and curvature effects.

Using the variables listed above and restricting attention to steady fully developed flow with a large Peclet number, the conservation equations can be written in non-dimensional form as follows:

continuity,

$$\frac{\partial}{\partial r}\Big(r(1+\delta r\cos\phi)u\Big)+\frac{\partial}{\partial\phi}\Big((1+\delta r\cos\phi)v\Big)=0 \tag{1}$$

r-momentum,

$$(\mathbf{u}\cdot\nabla)u-\frac{v^2}{r}-\frac{De^2w^2\cos\phi}{4(1+\delta r\cos\phi)}$$
$$=-\frac{Re^2}{4}\frac{\partial p}{\partial r}-Gr\frac{\mathbf{g}_r}{\mathbf{g}}T$$
$$+\left[\nabla^2u-\frac{2}{r^2}\frac{\partial v}{\partial\phi}-\frac{u}{r^2}+\frac{\delta v\sin\phi}{r(1+\delta r\cos\phi)}\right.$$
$$\left.+\frac{\delta^2\cos\phi}{(1+\delta r\cos\phi)^2}(v\sin\phi-u\cos\phi)\right] \tag{2}$$

ϕ-momentum,

$$(\mathbf{u}\cdot\nabla)v+\frac{uv}{r}+\frac{De^2w^2\sin\phi}{4(1+\delta r\cos\phi)}$$
$$=-\frac{Re^2}{4}\frac{1}{r}\frac{\partial p}{\partial\phi}-Gr\frac{\mathbf{g}_\phi}{\mathbf{g}}T$$
$$+\left[\nabla^2v+\frac{2}{r^2}\frac{\partial u}{\partial\phi}-\frac{v}{r^2}-\frac{\delta u\sin\phi}{r(1+\delta r\cos\phi)}\right.$$
$$\left.-\frac{\delta^2\sin\phi}{(1+\delta r\cos\phi)^2}(v\sin\phi-u\cos\phi)\right] \tag{3}$$

θ-momentum,

$$(\mathbf{u}\cdot\nabla)w+\frac{\delta w}{1+\delta r\cos\phi}(u\cos\phi-v\sin\phi)$$
$$=-\frac{1}{2(1+\delta r\cos\phi)}\frac{\partial p}{\partial\theta}+\nabla^2w-\frac{\delta^2w}{(1+\delta r\cos\phi)^2} \tag{4}$$

energy,

$$(\mathbf{u}\cdot\nabla)T=\frac{1}{Pr}\nabla^2T \tag{5}$$

where

$$(\mathbf{u}\cdot\nabla)=u\frac{\partial}{\partial r}+\frac{v}{r}\frac{\partial}{\partial\phi}$$

$$\nabla^2=\frac{1}{r(1+\delta r\cos\phi)}\left[\frac{\partial}{\partial r}\left(r(1+\delta r\cos\phi)\frac{\partial}{\partial r}\right)\right.$$
$$\left.+\frac{1}{r}\frac{\partial}{\partial\phi}\left((1+\delta r\cos\phi)\frac{\partial}{\partial\phi}\right)\right].$$

The small curvature approximation has not been made in the derivation of these equations. Note that equation (5) does not contain a streamwise diffusion term. Streamwise diffusion is negligible for the constant heat flux boundary conditions of the present study, regardless of Peclet number. The streamwise pressure gradient $(\partial P/\partial\theta)$ which appears in equation (4) is considered constant over the tube cross section. Although this assumption is often made in the literature without comment, it is not strictly correct for fully developed flows which are influenced by buoyancy. The streamwise temperature gradient results in streamwise density variations which, in turn, cause the pressure field to constantly readjust to the changing

weight of the fluid. This implies that the streamwise pressure gradient is a function of the cross-stream (r, ϕ) coordinates and thus is not constant. This streamwise pressure gradient variation can only be neglected when the cross-stream temperature and density gradients are much larger than the corresponding gradients in the streamwise direction. In order for this to be true, the Peclet number must be large. Thus, it is the assumption about the streamwise pressure gradient, rather than the neglect of streamwise energy diffusion, which results in the large Peclet number requirement.

In order to solve the conservation equations using the numerical solution procedure described below, boundary conditions for velocity and temperature are required at each boundary of the computational domain. The boundaries include the wall of the tube $(r = a)$ and the tube centerline $(r = 0)$. At the tube wall the no-slip and impermeability conditions apply for all velocity components. Conditions at the tube centerline are derived from equations (2) and (3) by taking the limit as $r \to 0$. When the limiting procedure is applied, only the viscous terms containing a $1/r^2$ remain, leading to [10]:

$$\frac{\partial^2 u}{\partial \phi^2} - 2\frac{\partial v}{\partial \phi} - u = 0$$

$$\frac{\partial^2 v}{\partial \phi^2} + 2\frac{\partial u}{\partial \phi} - v = 0.$$

Once periodicity is imposed, these equations have general solutions:

$$u = A(\theta)\cos\phi + B(\theta)\sin\phi,$$

$$v = -A(\theta)\sin\phi + B(\theta)\cos\phi.$$

The functions $A(\theta)$ and $B(\theta)$ are simply components of the velocity vector at the tube centerline and are obtained from the second of the two relations using calculated v-velocities near the centerline. Because of the staggered nature of the computational grid, only u-velocity information is needed at the centerline. This is obtained from the first of the two relations once $A(\theta)$ and $B(\theta)$ are known.

The energy boundary condition at the tube wall consists of a specified total cross-section heat flux. In addition, for condition 1 $(T_w = f(\theta))$, the tube wall temperature is held at a constant value at each cross-section which is elevated above the bulk fluid temperature in order to deliver the required heat. Mathematically condition 1 is stated as follows,

condition 1:

$$\int_0^{2\pi} q_w(\phi)(1 + \delta\cos\phi)\,d\phi = \text{const.} \quad T_w = f(\theta).$$

For condition 2, the tube wall heat flux is simply a constant which is not a function of either θ or ϕ,

$$\text{condition 2:} \quad q_w = \text{const.} \quad T_w = f(\theta, \phi).$$

3. NUMERICAL METHOD

The numerical procedure used in the present study has been described in Goering and Humphrey [11] and is briefly reviewed here. The procedure is based on the control volume approach and makes use of a staggered grid arrangement. The conservation equations are discretized by integrating them over the resulting control volumes in each of the three coordinate directions. Central differences are used to approximate the diffusion terms and the second order upstream interpolation method of Leonard [12] is employed for the convective terms. A Poisson-type equation for pressure is derived from a combination of the continuity and momentum equations. The resulting set of discrete algebraic equations were solved using an iterative technique. At the beginning of the iteration sequence an initial guess for the solution was supplied (typically taken from the final result of a calculation at a different *De–Gr* combination). The initial guess was gradually improved via the iteration sequence until the sum of the normalized residuals was reduced to less than 1×10^{-3} for each of the conservation equations. Testing indicated that further reductions in the size of the residuals had a negligible impact on the computed results.

A number of recent studies have examined the accuracy of the convective differencing technique employed in the present work; see, for example, Sharif and Busnaina [13] and Castro and Jones [14]. These studies have shown that the accuracy of the present scheme compares well with other high order convective differencing schemes, and that the present scheme is significantly more accurate than first-order upwind differencing.

Testing was performed prior to applying the procedure outlined above to the problems of concern to the present study. This was done to insure proper implementation of the conservation equations and to determine the influence of grid resolution on accuracy of the calculated results. Much of this testing effort has been discussed in detail in Goering and Humphrey [11] and is also reviewed in Goering [10]. In the following paragraphs we briefly discuss the test cases which relate directly to the fully developed flow calculations performed here.

Table 1 shows friction factor ratios for fully developed curved tube flow. The friction ratio is defined as the ratio of flow resistance in the curved

Table 1. Comparison of friction factor ratios with other numerical data

	Ref. [15]	Ref. [16]	Ref. [17]	Present work		
				f_c/f_s		
De		$\delta = 0$		$\delta = 0.05$	$\delta = 0.01$	$\delta = 0.002$
114	1.550	1.548	1.548	1.570	1.553	1.549
372	2.392	2.377	2.383	2.424	2.393	2.386

Table 2. Effect of grid refinement on friction factor ratios

De	f_c/f_s 38 × 18 grid	76 × 36 grid	% change
400	2.505	2.480	1.00
600	2.954	2.902	1.76

tube flow normalized by the Poiseuille flow resistance in a corresponding straight tube:

$$\frac{f_c}{f_s} = \frac{G_c}{G_s}. \tag{6}$$

In this expression G_c and G_s are the streamwise pressure gradients for the curved tube flow and the Poiseuille flow, respectively. $G_s = 32\bar{w}\mu/d^2$ and G_c is calculated directly by the numerical procedure. Each of the numerical studies of Collins and Dennis [15], Dennis and Ng [16] and Yang and Keller [17] have examined curved tube flow in the limit as $\delta \to 0$ for Dean numbers of 114 and 372. Table 1 includes friction ratios taken from each of these studies in addition to friction ratio calculated with the present numerical procedure for $\delta = 0.05$, 0.01, and 0.002. In the limit as $\delta \to 0$ the present results agree quite well with the other data.

A final series of tests was performed in order to investigate the influence of grid resolution on the results of the present flow configurations. This was accomplished by examining high Dean number flow in a curved tube without buoyancy. Calculations were carried out for Dean numbers of 400 and 600 using grids with 38 × 18 and 76 × 36 unevenly spaced nodes. Friction ratios for these calculations are shown in Table 2. Even at these relatively high Dean numbers there is less than a 2% difference in the friction ratios for the two grids. In conjunction with this grid resolution test we also periodically checked the results which are presented in Section 4 by repeating calculations on finer grids. The results presented in Section 4 were obtained with a 38 × 18 grid (38 nodes in the circumferential and 19 in the radial directions). The adequacy of the 38 × 18 grid was reconfirmed by periodically repeating calculations on a 50 × 22 node grid. In all cases the friction factor and Nusselt number data differed by less than 2% for these grids.

4. RESULTS AND DISCUSSION

We first present the results for thermal boundary conditions 1 and 2 in the range of dual influence. Secondly, accurate bounds are established for the region of dual influence for both conditions. The regime map for condition 1 ($T_w = f(\theta)$) is compared with data from the existing literature. For condition 2 ($T_w = f(\theta, \phi)$) we also present the boundary of a region in De–Gr parameter space where we were unable to find fully developed solutions. Friction factor and Nusselt number results were obtained and were used to construct plots which show the effects of curvature and buoyancy. Selected velocity and temperature contour plots are also presented.

All of the results presented were obtained with the Prandtl number and curvature ratio equal to 1 and 0.05, respectively. Numerous studies have shown that the Dean number and the curvature ratio are important as separate parameters for characterizing the influence of curvature on flow through tubes with finite curvature ratios; see the review of Berger *et al.* [18] for a discussion of this issue. However, it is well known that the influence of the curvature ratio is small for $\delta \leqslant 0.05$. The friction factor ratio for curved tube flow changes by less than 2% as δ varies from 0.05 to 0.002 (Table 1). Thus, the results presented in the following sections should apply to all flow configurations with $\delta \leqslant 0.05$, these being completely characterized by the Dean and Grashof numbers.

4.1. *Boundary condition* 1 ($T_w = f(\theta)$)

Figure 2 summarizes the friction factor results which were obtained for boundary condition 1. These results are presented in terms of the friction factor in the heated curved tube normalized by the Poiseuille flow friction factor. Friction factor ratios are presented for Dean numbers of 0, 50, 100, 200, 400 and 600 at Grashof numbers which range from 10^3 to 10^7. The results for $De = 0$ represent the limiting condition for no curvature influence. For $De > 0$, the friction ratio curves consist of a portion that is first independent of Gr (for small Gr) which then increase with increasing Gr to the bounding $De = 0$ curve. Thus, at a given Dean number, there is a certain Grashof number below which the effects of buoyancy are unimportant. At high Gr, all the curves asymptotically approach the $De = 0$ curve, and the effect of curvature (Dean number) is no longer important. When buoyancy becomes important at a given Dean number, its effect is to increase the friction factor ratio. This occurs because the influence of buoyancy is to increase the

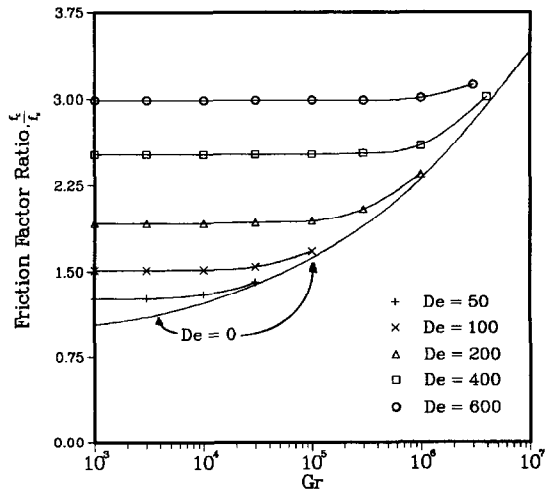

Fig. 2. Friction factor ratios for fully developed heated curved tube flow with boundary condition 1 ($T_w = f(\theta)$).

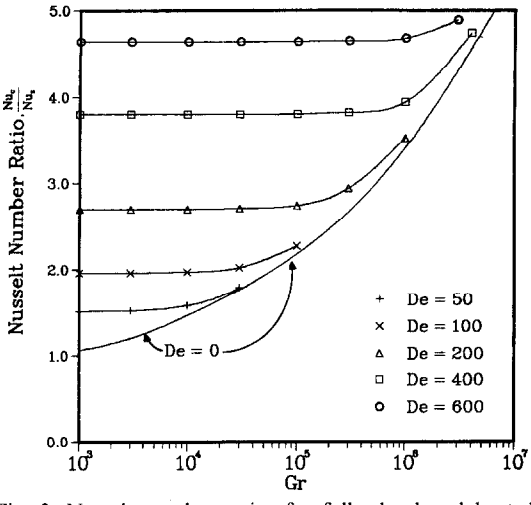

Fig. 3. Nusselt number ratios for fully developed heated curved tube flow with boundary condition 1($T_w = f(\theta)$).

values of the secondary velocities which augments momentum transport and increases the friction.

Figure 3 displays Nusselt number ratios for boundary condition 1. The Nusselt number ratio is given by:

$$\frac{Nu_c}{Nu_s} = \frac{\dfrac{2aq_w}{k(T_w - T_b)}}{Nu_s} \tag{7}$$

where Nu_s is the Nusselt number of a forced convection (non-buoyant) Poiseuille flow for constant wall heat flux (4.364). Figure 3 shows trends very similar to those of Fig. 2 for the friction factor ratio. As before, the $De = 0$ curve is based on data for heated straight tubes without curvature effects. A comparison of Figs. 2 and 3 reveals that the increases in heat transfer are significantly larger than the corresponding increases in friction for given conditions. This is due to the fact that the heat transfer characteristics depend directly on both the velocity and the temperature profiles while the frictional characteristics are a function of the velocity profile only. The gradients of both streamwise velocity and temperature increase at the tube wall as *De* and/or *Gr* are increased.

Figures 4 and 5 show cross-stream velocity vectors, streamwise velocity contours, and temperature contours for boundary condition 1. These figures are oriented in the same manner as Fig. 1, with inner, outer, top, and bottom corresponding to $\phi = 180°$, $\phi = 0°$, $\phi = 90°$, $\phi = 270°$, respectively. Figure 4 is for Dean and Grashof numbers of 100 and 5×10^4, respectively, while Fig. 5 is for 400 and 2×10^6. Note that for these pairs of parameter values, Gr/De^2 is 5 and 12.5, respectively. Both of these Dean–Grashof number combinations fall in the middle of the region of dual curvature/buoyancy influence. The dual influence is illustrated quite well in Figs. 4(a) and 5(a) which show that the secondary flow travels downward in the region around the pipe centerline at an angle of $\phi \approx 315°$. In both cases it is apparent that there is no plane of flow symmetry. The vortices which appear in the upper portion of the tube cross section are more rounded in shape, while those in the lower portion are extended along the tube wall. This is particularly true for the higher parameter values illustrated in Fig. 5. Figure 5 also shows that the high *De–Gr* case yields more intense, thinner boundary layers along the tube walls. In both cases the streamwise velocity maximum and temperature minimum are located near the point where the cross-stream flow impinges on the tube wall, again at an angle of $\phi \approx 315°$.

4.2. *Boundary condition* 2 ($T_w = f(\theta, \phi)$)

Figure 6 summarizes the friction factor results which were obtained for boundary condition 2. As for boundary condition 1, all the data were obtained for $Pr = 1$ and are displayed for Dean numbers of 0, 50, 100, 200, 400 and 600, with the $De = 0$ results again corresponding to straight-tube values. For the range where buoyancy is important, boundary condition 2 results in friction factor ratios which are lower than for the corresponding condition 1 cases. This is reflected by the fact that the $De = 0$ line in Fig. 6 yields lower friction ratios than the corresponding line in Fig. 2. For $De > 0$, the friction factor ratios appearing in Figs. 2 and 6 are identical until buoyancy becomes important at the larger Grashof numbers. This is due to the fact that the temperature boundary conditions do not affect the friction factor ratio as long as buoyancy does not alter the cross-stream flow.

Comparing Figs. 2 and 6 illustrates the large differences between the solutions for conditions 1 and 2. The most dramatic difference is the large region of no fully-developed solutions shown in Fig. 6 for condition 2. Also, the effect of buoyancy for condition 2 is actually to *reduce* the friction factor ratio relative to the forced convection (curvature only) case. This is opposite to the behavior observed for boundary condition 1.

Within the region which is labeled 'no solution' in Fig. 6, it was not possible to find fully developed flow solutions with the two-dimensional calculation procedure. Several steps were taken to insure that lack of convergence was not due to a numerical instability (Goering [10]). The no solution region extends to relatively low values of the Dean number (less than 200) and of the Grashof number (slightly above 10^5). At these Dean and Grashof numbers, the numerical procedure has proven its numerical stability for other cases (e.g. Type 1 boundary conditions). It is suggested that the no-solution boundary corresponds to the onset of a physical instability which prevents a fully developed two-dimensional flow field from developing. In fact, in Goering [10], it is shown that the fully-developed solution is three-dimensional within this parameter range and displays a periodic waviness as the flow progresses downstream.

Figure 6 shows that (for $De > 0$) the effect of buoyancy for boundary condition 2 is to reduce the friction

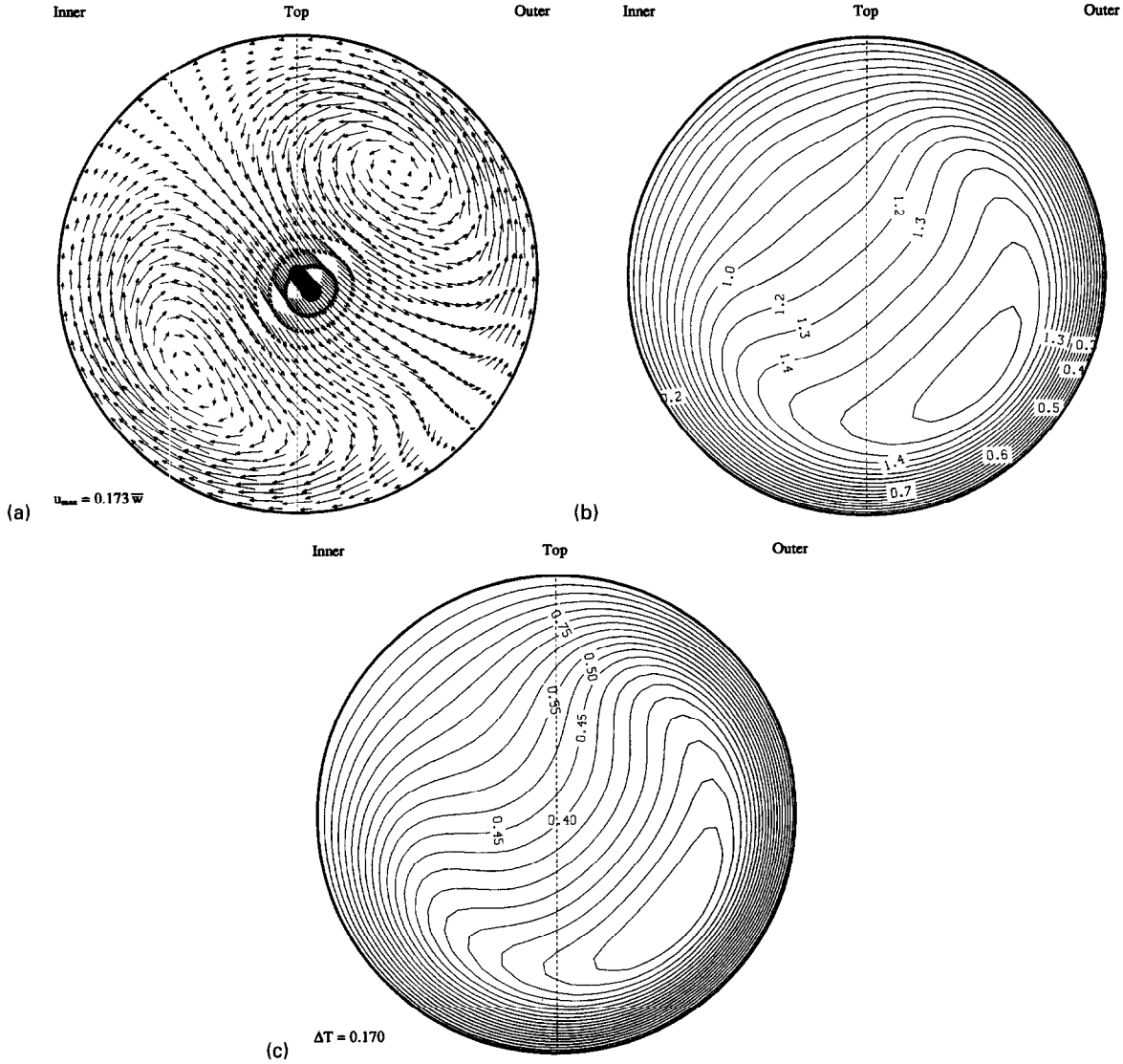

Fig. 4. Fully developed flow in a heated curved tube with boundary condition 1 ($T_w = f(\theta)$), $De = 100$, $Gr = 5 \times 10^4$: (a) cross-stream velocity; (b) streamwise velocity contours; (c) temperature contours.

factor ratio below the value when only the curvature influence is present. This result was somewhat unexpected since buoyancy would normally augment the cross-stream flow, thereby increasing momentum transport and increasing the friction factor. In fact, the results shown for $De = 0$ in the figure indicate that an increase in the friction ratio is observed as the Grashof number increases. Examination of the flow field results, to be presented in Figs. 8 and 9 for the type 2 boundary condition, shows that the motion in the upper portion of the tube cross section consists of a relatively stable stratified flow. It appears that the first influence of buoyancy under type 2 conditions is to produce a relatively stable warm flow in the upper portion of the cross section, and consequently, to reduce the overall cross-stream circulation. For this reason the friction factor is reduced as buoyancy becomes important in curved tube flow when boundary condition 2 is imposed.

Figure 7 displays Nusselt number ratios for boundary condition 2. The reduction in heat transfer caused by the buoyancy-induced stable stratification is much more pronounced than the friction factor results. Comparing Figs. 3 and 7 shows that the low Grashof number limit of the Nusselt number ratio is not the same for conditions 1 and 2. Interestingly, the Nusselt number for the type 2 condition is slightly higher than for the type 1 condition when only curvature is important (i.e. forced convection conditions).

Figures 8 and 9 show cross-stream velocity vectors, streamwise velocity contours, and temperature contours for boundary condition 2. Figure 8 corresponds to Dean and Grashof numbers of 100 and 5×10^4, respectively, while Fig. 9 corresponds to 400 and

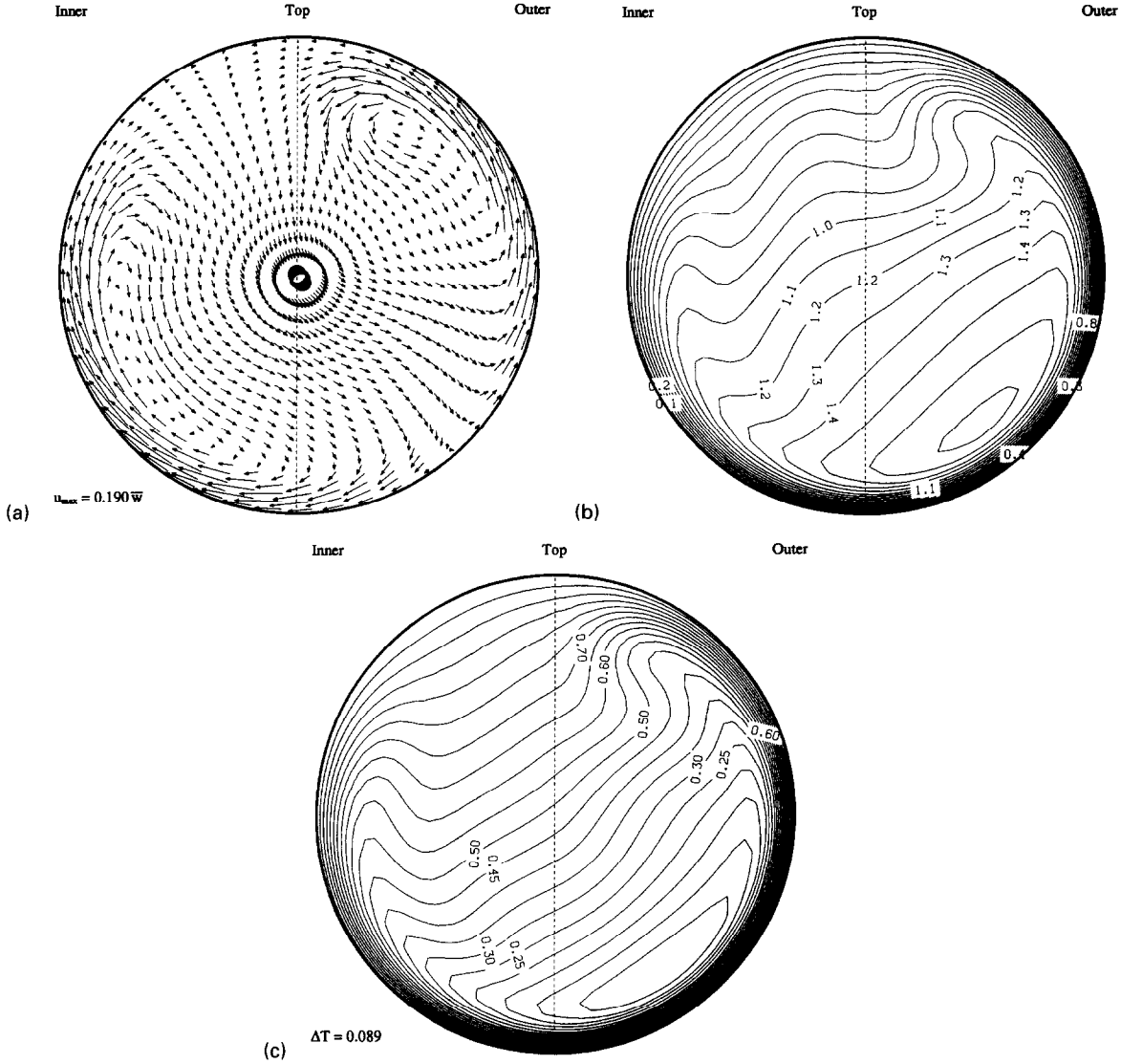

Fig. 5. Fully developed flow in a heated curved tube with boundary condition 1 ($T_w = f(\theta)$), $De = 400$, $Gr = 2 \times 10^6$: (a) cross-stream velocity; (b) streamwise velocity contours; (c) temperature contours.

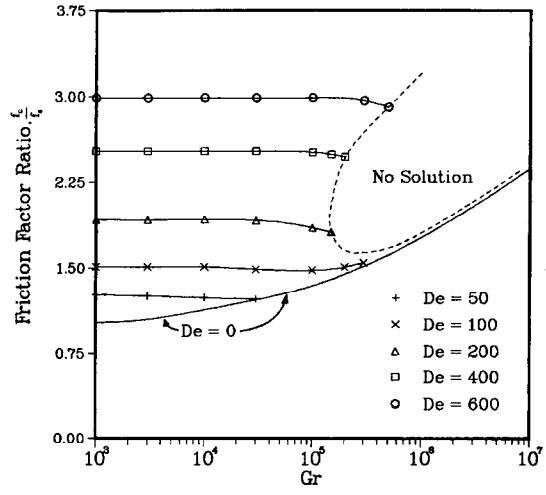

Fig. 6. Friction factor ratios for fully developed heated curved tube flow with boundary condition 2 ($T_w = f(\theta, \phi)$).

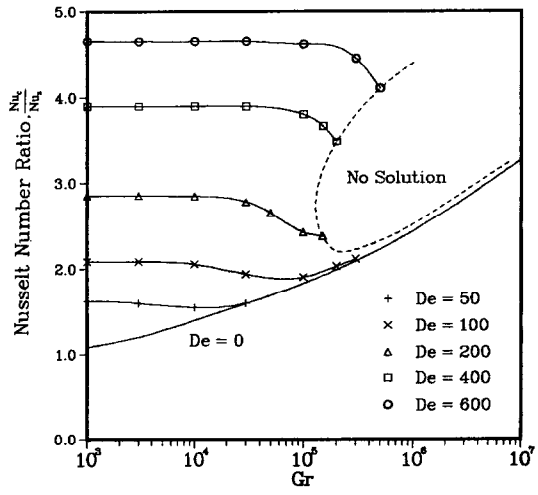

Fig. 7. Nusselt number ratios for fully developed heated curved tube flow with boundary condition 2 ($T_w = f(\theta, \phi)$).

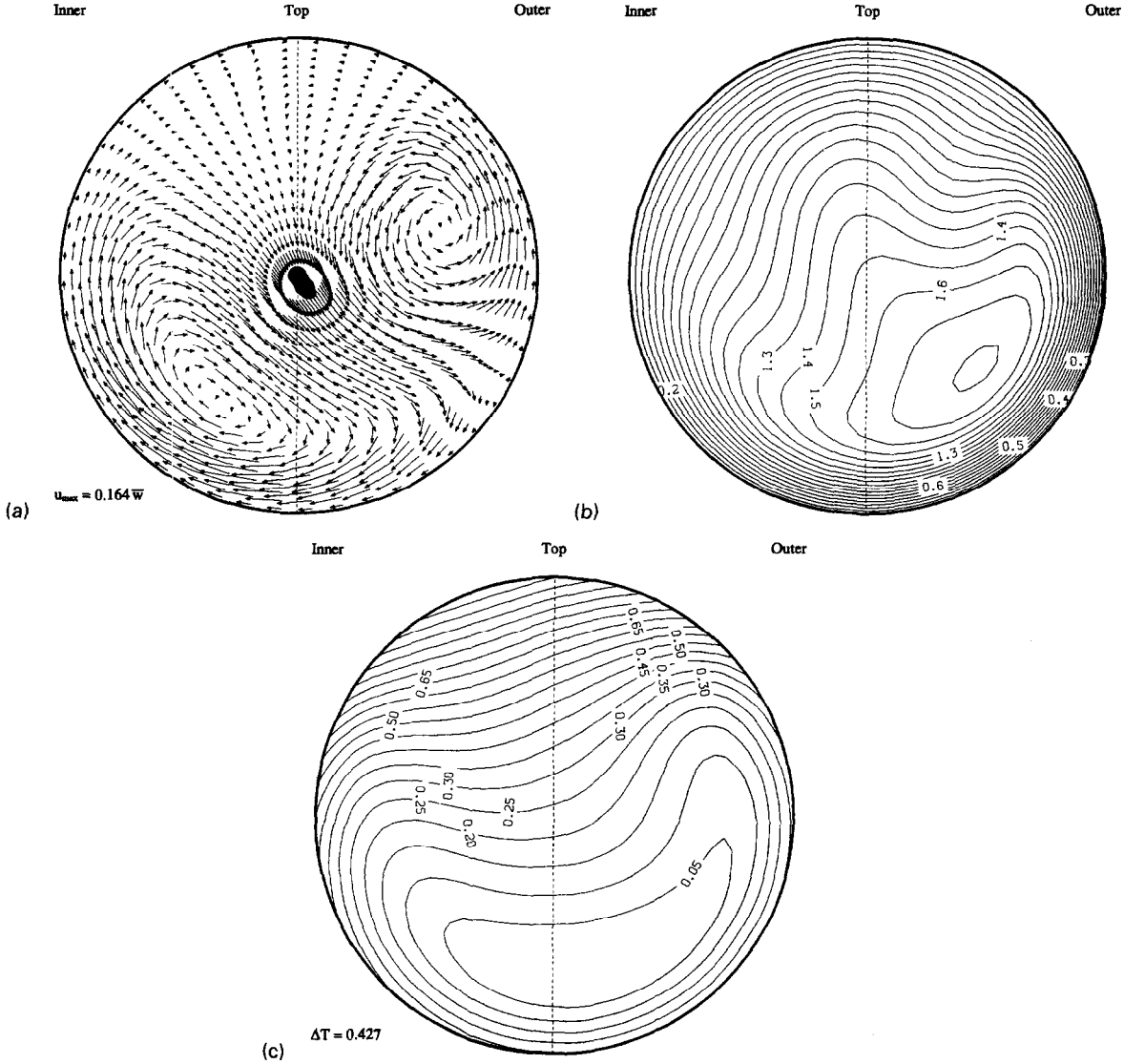

Fig. 8. Fully developed flow in a heated curved tube with boundary condition 2 ($T_w = f(\theta, \phi)$), $De = 100$, $Gr = 5 \times 10^4$: (a) cross-stream velocity; (b) streamwise velocity contours; (c) temperature contours.

2×10^5. The first of these Dean-Grashof number ratios falls in the middle of the dual curvature/buoyancy region with a Gr/De^2 ratio of 5. Note that when $De = 100$ there is no difficulty finding solutions, even at large Grashof numbers. The second Dean-Grashof number ratio is at the border of the no-solution region with $Gr/De^2 = 1.25$ (an order of magnitude less than the $De = 400$, $Gr = 2 \times 10^6$ pair used for condition 1 in Fig. 5, where curvature is more important than buoyancy).

Figure 8(a) shows that the cross-stream flow is weak in the upper portion of the tube cross section and that the two vortices which appear are highly asymmetric. In fact, the upper vortex is almost circular in shape, whereas the lower vortex is elongated along the tube wall. Comparison of Fig. 8(b) and (c) illustrates the large difference between the streamwise velocity and temperature fields for the type 2 boundary condition. For boundary condition 1 shown in Figs. 4 and 5 these fields were very similar. The essential difference between these two conditions is that condition 2 allows a peripheral wall temperature variation. As shown in Figs. 8(c) and 9(c), this peripheral wall temperature variation can be quite substantial and thus has a large impact on the resulting temperature profiles and the other flow variables. Figure 8(c) illustrates the stable temperature stratification which occurs in the upper portion of the tube cross section due to the high wall temperatures there.

In Fig. 9(a) the boundary fluid which flows along the top surface of the tube descends (after crossing the vertical centerline) towards the tube center. Figure 9(c) shows that large temperature gradients arise in this region. It is also apparent that the coldest fluid in the cross stream is located near the top of the cross section and is adjacent to the hottest region of the

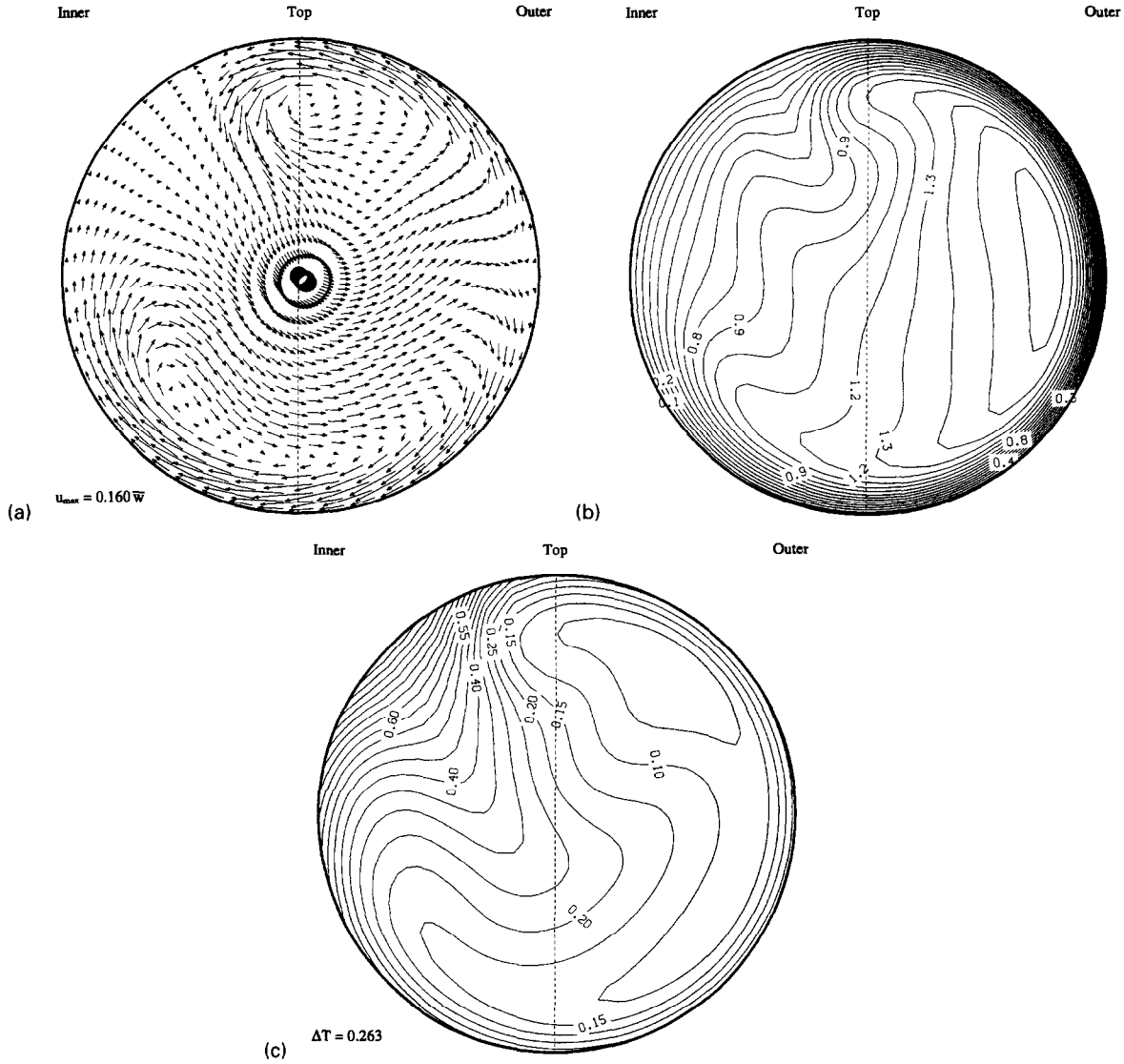

Fig. 9. Fully developed flow in a heated curved tube with boundary condition 2 ($T_w = f(\theta, \phi)$), $De = 400$, $Gr = 2 \times 10^5$: (a) cross-stream velocity; (b) streamwise velocity contours; (c) temperature contours.

flow. The proximity of the cold and hot fluid in this region is probably responsible for the instability which sets in at slightly larger Grashof numbers. In Fig. 9(b) it is evident that the curvature influence is relatively stronger for this parameter set than for the others examined. The streamwise velocity profiles display their maximum values in the outer portion of the tube cross section at an angle of $\phi \approx 0°$, as expected in a curvature-dominated flow.

4.3. *Regime maps*

The final topic relating to fully developed flows in heated curved tubes concerns the region of dual curvature/buoyancy influence. The studies by Prusa and Yao [6], Lee *et al.* [7] and Futagami and Aoyama [8] have each examined this issue for boundary condition 1 ($T_w = f(\theta)$). Results from these studies are summarized in Fig. 10. Three regions are identified in the figure and are labeled I, II, and III. These regions correspond to forced convection (only curvature important), mixed convection (both curvature and buoyancy important), and free convection (only buoyancy important), respectively. The curves which are shown in the figure are the boundaries which separate the regions, as reported in the studies mentioned above. The boundary between regions I and II is obtained by gradually increasing the Grashof number (with *De* fixed) until the Nusselt number varies by a prescribed amount from the pure forced convection result. For the studies of Prusa and Yao, and Lee *et al.*, a 5% change was taken as the demarcation, whereas Futagami and Aoyama used a 2% change. The boundary separating regions II and III is obtained in a similar manner. An obvious conclusion to be drawn

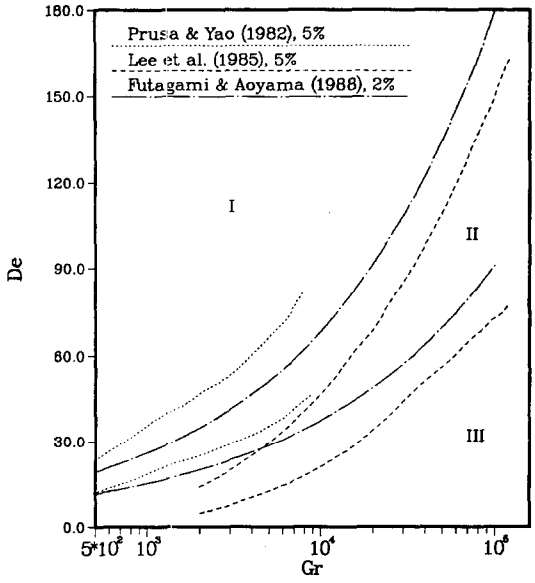

Fig. 10. Regime map for fully developed heated curved tube flow with boundary condition 1 ($T_w = f(\theta)$). Results from the literature.

from Fig. 10 is that the literature is in disagreement concerning the value of the parameters for which curvature and/or buoyancy are important in heated curved tube flow. Note that, since the data presented by Futagami and Aoyama are more sensitive (2% limit), these curves should fall outside the curves of the other two studies, but this is not the case. In fact, the studies of Prusa and Yao and of Lee *et al.* are in complete disagreement concerning the location of region II. Region II as reported by Futagami and Aoyama overlaps a portion of the region II reported in the other two studies.

A careful comparison of the parameters is in order. In each of the studies the curvature influence is characterized by the Dean number as defined in the present work (referred to as k in Prusa and Yao).

Unfortunately, the situation is somewhat more complicated for the buoyancy characterization. The studies of Prusa and Yao and Futagami and Aoyama use a combination of the Reynolds and Rayleigh numbers to characterize buoyancy, whereas the study of Lee *et al.* and the current study use a Grashof number for this purpose. The relation between the Reynolds number of Prusa and Yao and that used in the current work is:

$$Re_{P-Y} = Re\frac{f_c}{f_s} \tag{8}$$

where f_c/f_s is the friction factor ratio under the given flow conditions. The following relation is useful:

$$(ReRa)_{P-Y} = \frac{f_c}{f_s}\frac{\beta g \tau a^4}{\nu^2} RePr = 2\frac{f_c}{f_s} Gr \tag{9}$$

where Gr is the Grashof number used in this study. Because of the Reynolds number used by Prusa and Yao, it is necessary to know the frictional characteristics of the flow under each flow condition to determine the Grashof number and these data were presented by them. In the study of Lee *et al.* The following Grashof number is used:

$$Gr_L = \frac{\beta g q_w a^4}{\nu^2 k} = \tfrac{1}{2} Gr \tag{10}$$

which is half the value used in the current study. Futagami and Aoyama use a combination of Reynolds and Rayleigh numbers to characterize buoyancy. Their Reynolds number definition coincides with that used in the present study, and:

$$(ReRa)_{F-A} = \frac{\beta g \tau a^4}{\nu^2} RePr = \tfrac{1}{2} Gr. \tag{11}$$

Equations (8)–(11) were used in constructing Fig. 10.

Figure 11 is identical to Fig. 10 with the addition of the results from the present study. The present results correspond to a 5% limit and, therefore, are directly comparable to the data of Prusa and Yao and Lee *et al.* They suggest a somewhat smaller mixed convection region (region II) than obtained in the studies of Prusa and Yao and Lee *et al.* Agreement between the results of Prusa and Yao, Lee *et al.* and the present study is generally poor. An exception is the upper limit of Lee *et al.*, which agrees exactly with that found in the current study in the region $2 \times 10^4 < Gr < 1 \times 10^5$. Region II, as delineated by the current study, reduces to a point at low Dean and Grashof numbers. This reflects the fact that at low Dean and Grashof numbers neither curvature nor buoyancy are capable of producing a 5% increase in heat transfer over the straight pipe non-buoyant flow. This point occurs at values of the Dean and Grashof

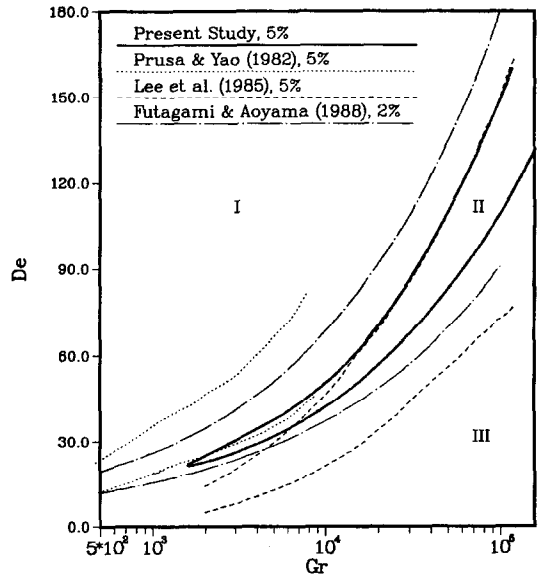

Fig. 11. Regime map for fully developed heated curved tube flow with boundary condition 1 ($T_w = f(\theta)$). Comparison of current results with results from the literature.

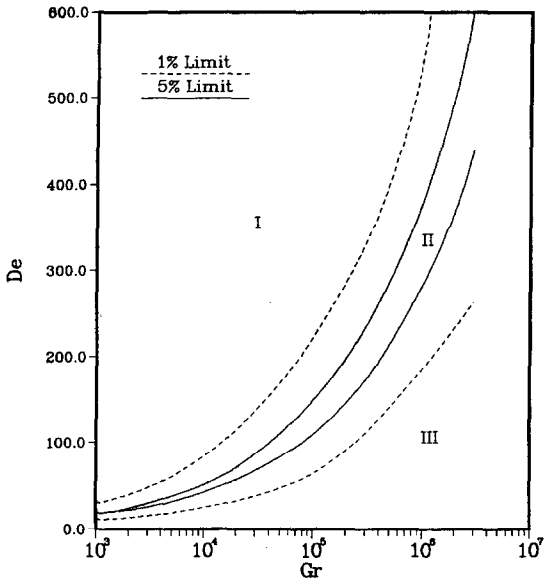

Fig. 12. Regime map for fully developed heated curved tube flow with boundary condition 1 ($T_w = f(\theta)$). Results from the present study.

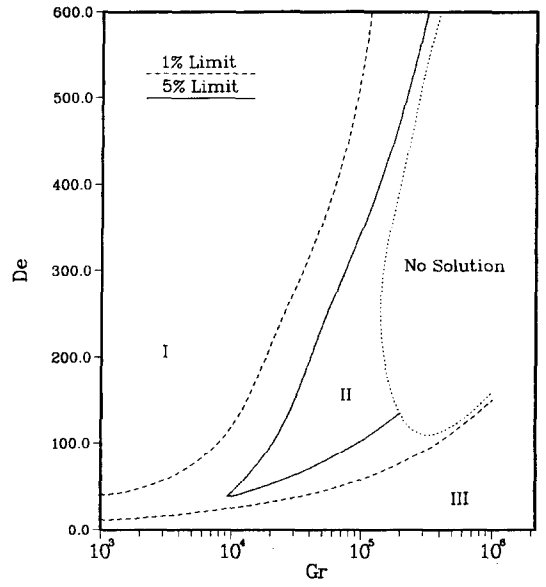

Fig. 13. Regime map for fully developed heated curved tube flow with boundary condition 2 ($T_w = f(\theta, \phi)$). Results from the present study.

numbers of about 20 and 1.5×10^3, respectively. The studies of Prusa and Yao and Lee *et al.* do not appear to yield this result.

Agreement between the results of the present study and those of Futagami and Aoyama is much better. Figure 11 shows that the 2% limits of Futagami and Aoyama do bracket the results of the current study (5% limits) as they should.

The effect of different limits is shown in Fig. 12 which displays results from the current study for both 5% and 1% limits. This figure also extends the results of Fig. 11 to larger Dean and Grashof numbers. There is a significant difference between the 1% and 5% limits. The combination of Figs. 11 and 12 indicates that the current results are in good agreement with the study of Futagami and Aoyama and are in good agreement with the upper limit presented by Lee *et al.* for $Gr > 2 \times 10^4$.

Figure 13 displays the heat transfer regimes for boundary condition 2 ($T_w = f(\theta, \phi)$). Both the 1% and 5% limits are shown and regions I, II, and III correspond to forced, mixed, and free convection as before. Currently, no results are available in the literature for this boundary condition. The region of Dean–Grashof number space in which no two-dimensional fully developed solutions could be found has been marked with a dotted line in the figure. The lower limits of region II which are shown in Fig. 13 are approximately the same as those for boundary condition 1 which were displayed in Fig. 12. The upper limits, however, are at significantly lower Grashof numbers for a given Dean number. This results in a much larger mixed convection region for condition 2 than was observed for the type 1 condition. Note also that the upper limits actually correspond to a decrease in the Nusselt number (1% or 5%) from the pure convection results. The lower limit in Fig. 13 and both the upper and lower limits in Figs. 11 and 12 correspond to increases in the Nusselt number.

5. CONCLUSION

The characteristics of fully-developed heated curved tube flow have been investigated in the range of dual curvature/buoyancy influence. Results were obtained from numerical solutions of the Navier–Stokes and energy equations for fully-developed flow conditions. Two types of thermal boundary conditions were examined; one consisting of a uniform cross-sectional heat flux with constant peripheral tube wall temperature (type 1) and the other being a constant peripheral heat flux (type 2). For both cases flow friction and heat transfer results have been presented in terms of friction factor and Nusselt number ratios. For boundary condition 2, a large region was found in the *De–Gr* parameter space where no fully developed solutions could be found. Regime maps are presented for both conditions which delineate the region of dual curvature/buoyancy influence in *De–Gr* parameter space. Disagreements amongst previous studies with regard to the region of dual curvature/buoyancy influence for condition 1 ($T_w = f(\theta)$) are discussed in relation to the new data.

REFERENCES

1. Dean, W. R., Note on the motion of fluid in a curved pipe. *Philosophy Magazine*, 1927, **20**, 208–223.
2. Dean, W. R., The streamline motion of fluid in a curved pipe. *Philosophy Magazine*, 1928, **30**, 673–693.
3. Morton, B. R., Laminar convection in uniformly heated horizontal pipes at low Rayleigh numbers. *Quarterly Journal of Mechanics and Applied Mathematics*, 1959, **11**, 410–420.

4. Cheng, K. C. and Yuen, F. P., Flow visualization experiments on secondary flow patterns in an isothermally heated curved pipe. *Journal of Heat Transfer*, 1987, **109**, 55–61.
5. Yao, L. S. and Berger, S. A., Flow in heated curved pipes. *Journal of Fluid Mechanics*, 1978, **88**, 339–354.
6. Prusa, J. and Yao, L. S., Numerical solution for fully developed flow in heated curved tubes. *Journal of Fluid Mechanics*, 1982, **123**, 503–522.
7. Lee, J., Simon, H. A. and Chow, J. C. F., Buoyancy in developed laminar curved tube flows. *International Journal of Heat & Mass Transfer*, 1985, **28**, 631-640.
8. Futagami, K. and Aoyama, Y., Laminar heat transfer in a helically coiled tube. *International Journal of Heat & Mass Transfer*, 1987, **31**, 387–396.
9. Newell, P. H. and Bergles, A. E., Analysis of combined free and forced convection for fully-developed laminar flow in horizontal tubes. *Journal of Heat Transfer*, 1970, **92**, 83–89.
10. Goering, D. J., The influence of curvature and buoyancy in three-dimensional pipe flows. Ph.D. thesis, University of California, Berkeley, 1989.
11. Goering, D. J. and Humphrey, J. A. C., On the stability of tube flows subject to body forces. *Physics of Fluids A*, 1993, **5**, 3107–3121.
12. Leonard, B. P., A stable and accurate convective modeling procedure based on quadratic upstream interpolation. *Computational Methods in Applied Mechanical Engineering*, 1979, **19**, 59–98.
13. Sharif, M. A. R. and Busnaina, A. A., Assessment of finite difference approximations for the advection terms in the simulation of practical flow problems. *Journal of Computational Physics*, 1988, **74**, 143–176.
14. Castro, I. P. and Jones, J. M., Studies in numerical computations of recirculating flows. *International Journal of Numerical Methods in Fluids*, 1987, **7**, 793–823.
15. Collins, W. M. and Dennis, S. C. R., The steady flow of a viscous fluid in a curved pipe. *Quarterly Journal of Mechanics and Applied Mathematics*, 1975, **28**, 133–156.
16. Dennis, S. C. R. and Ng, M., Dual solutions for steady laminar flow through a curved tube. *Quarterly Journal of Mechanics and Applied Mathematics*, 1981, **35**, 305–324.
17. Yang, Z. and Keller, H. B., Multiple laminar flows through curved pipes. *Applied Numerical Mathematics*, 1986, **2**, 257–271.
18. Berger, S. A., Talbot, L. and Yao, L. S., Flow in curved pipes. *Annual Review of Fluid Mechanics*, 1983, **15**, 461–512.